J. Phys. B: At. Mol. Opt. Phys. **27** (1994) 241–256. Printed in the UK

Photoionization of Kr near 4s threshold: II. Intermediate-coupling theory

V L Sukhorukov†, B M Lagutin†, I D Petrov†, H Schmoranzer‡, A Ehresmann‡ and K-H Schartner§

† Institute of Physics, Rostov University, Rostov-on-Don 344104, Russian Federation
‡ Fachbereich Physik, Universität Kaiserslautern, D-67653 Kaiserslautern, Federal Republic of Germany
§ I. Physikalisches Institut, Universität Giessen, D-35392 Giessen, Federal Republic of Germany

Received 21 June 1993, in final form 22 September 1993

Abstract. The Kr 4s-electron photoionization cross section as a function of the exciting-photon energy in the range between 30 eV and 90 eV was calculated using the configuration interaction (CI) technique in intermediate coupling. In the calculations the 4p spin–orbital interaction and corrections due to higher orders of perturbation theory (the so-called Coulomb interaction correlational decrease) were considered. Energies of Kr II states were calculated and agree with spectroscopic data within less than 10 meV. For some of the Kr II states new assignments were suggested on the basis of the largest component among the calculated CI wavefunctions.

1. Introduction

The interaction of the Kr atom with photons of an energy near the 4s threshold is of essentially many-electron nature which has consequences on several features of the atoms: the removal of the 4s electron strongly polarizes the 4p shell (see e.g. Sukhorukov *et al* 1991, Petrov and Sukhorukov 1991). Furthermore, the removal of a 4p electron is accompanied by removal of a 4s electron (intershell correlation, Amusia and Cherepkov 1975) and excitations of additional 4p electrons into unoccupied discrete states (satellite-level excitations, Sukhorukov *et al* 1991). Finally the autoionization of atomic resonances has a strong influence on the various satellite cross sections and the 4s-electron ionization cross section (see e.g. Schmoranzer *et al* 1990, Hall *et al* 1990).

Recently absolute values of satellite-state cross sections were measured by photon-induced fluorescence spectroscopy (PIFS) and also calculated (Schmoranzer *et al* 1993). From the theoretical point of view the 4p spin–orbital interaction has not yet been considered as well as corrections due to higher orders of perturbation theory (PT) (the so-called Coulomb interaction correlational decrease). In this paper the theory will be improved by considering these two points.

Section 2 contains the description of the theory and possible applications. The results of the calculations and their comparison with available experimental and earlier theoretical data are presented in section 3. The most significant final results and conclusions are collected in section 4.

0953-4075/94/020241+16$07.50

2. Theory

For the calculation of photoionization cross sections of the Kr II $4s^{-1}$ state and Kr II $4p^{-2}nl$ satellite states it is necessary to know the total wavefunctions and energies of the initial and final atomic states. In the present paper the calculation of the initial state (i.e. the ground state of Kr I) was carried out using many-body PT. Energies and wavefunctions of the final states were calculated in the frame of both PT and the theory of configuration interaction (CI).

In this section some features of the present calculations will be described. The accuracy of the final ionic-state energies and wavefunctions will be demonstrated by comparison of calculated and measured energy levels and radiative branching ratios of selected states which decay purely by radiation.

2.1. Atomic energies and total wavefunctions

The zero-order wavefunctions and virtual orbitals were calculated in the non-relativistic Hartree–Fock (HF) approximation. For this purpose the following integro–differential equation for the radial part was solved for each relevant configuration (see below)

$$(h_l(I) - \varepsilon_{nl})P_{nl}(r) = 0. \tag{1}$$

Here $h_l(I)$ denotes the single-electron HF operator averaged over the configuration I. The radial parts of wavefunctions for single-electron virtual states were also obtained by solving (1) in the frozen-core approximation with an additional 4p vacancy. Relativistic corrections in Breit form (Bethe and Salpeter 1957) have been included (see also Schmoranzer *et al* 1993). The differences $E(I, 0)$ between the HF energies of excited Kr configurations $E(I)$ and the Kr ground state E_0 are shown in table 1.

In the next step the subsets of strongly and weakly interacting configurations were determined by evaluating the parameter

$$\frac{|\langle Im_I|V|Xm_X\rangle|^2}{E_0(I) - E_0(X)} \tag{2}$$

where I, X are the considered configurations, m_I and m_X are both the total and intermediate momenta of the I and X configurations, respectively, $E_0(I)$, $E_0(X)$ are the averaged HF energies of the configurations I, X and $V = H - H_0$ (H being the total Hamiltonian and H_0 being the zero-order Hamiltonian used in (1)).

The subset of strongly interacting configurations for the initial state of Kr I consists of only one configuration, i.e. the ground state configuration. For the final ionic configurations this subset was determined as consisting of $4s^{-1}$, $4p^{-2}nd$ ($n = 4, 5, 6, 7, 8, \varepsilon$) and $4p^{-2}ns$ ($n = 5, 6, \varepsilon$) where ε denotes continuum configurations.

The terms of these configurations were used to form the basis of a CI secular matrix whose elements $E(IM_I, Km_K)$ were calculated by the formula

$$E(Im_I, Km_K) = E \cdot \delta(I, K) + \langle Im_I|V|Km_K\rangle \tag{3}$$

where the designations are as in (2), $\delta(I, K)$ is the Kronecker symbol and E is the corrected average configuration energy (see below).

The continuum states in the matrix representation (3) were included in a quasi-discrete manner (Demekhin *et al* 1979). Before diagonalizing the secular matrix the following corrections have been made.

The energies of the set of strongly interacting configurations were corrected with respect to the set of weakly interacting configurations according to the second order of PT (Rajnak and Wybourne 1963, Demekhin *et al* 1979):

$$\Delta E(I)=\frac{1}{g(I)}\sum_{X}\frac{\sum_{m_X m_I}|\langle Im_I|V|Xm_X\rangle|^2}{E(I)-E(X)} \tag{4}$$

where $g(I)$ is the statistical weight of the I-configurations. Summation is performed over discrete states Xm_X and integration over continuum states Xm_X. $E(I)$ and $E(X)$ denote the average energies of the I and X configurations, respectively. These average energies have been taken instead of $E(Im_I)$, $E(Xm_X)$, because for weakly interacting states the energy difference $E(I)-E(X)$ is much greater than the energy splitting between the Im_I, Xm_X states within the I, X configurations. The corrections (4) are calculated for all configurations X which can be obtained when one or two core electrons move into unoccupied core states or virtual {s}, {p}, {d}, {f}, {g}, {h} channels. For each channel the two lowest lying discrete states and continuum states in the energy range between 0 and 400 Ry were considered.

Higher order PT corrections E_{HO} were included also as described and calculated in the preceding paper (Schmoranzer *et al* 1993). The corrected average configuration energies are also presented in table 1.

Table 1. Calculated average configuration energies of Kr II states.

Conf. (I)	$E(I, O)$[a] (eV)	$E_{corr}(I, O)$[b] (eV)
$4s^{-1}$	30.97	30.86
$4p^{-2}4d$	29.69	31.08
$4p^{-2}5d$	33.42	35.28
$4p^{-2}6d$	34.97	36.89
$4p^{-2}7d$	35.78	37.70
$4p^{-2}8d$	36.25	38.17
$4p^{-2}5s$	27.73	29.16
$4p^{-2}6s$	32.72	34.64
$4p^{-2}$	37.39	39.31

[a] Difference of HF energies of configurations I and the HF energy of the Kr I ground state $E_0^{Breit}=-5573.218$ Ry.

[b] Energy differences with corrected I configuration energies: $E_{corr}(I, O)=E(I, O)+\Delta E(I)+E_{HO}$ (see text).

Analogously to (4) corrections to the non-diagonal matrix elements $\langle Im_I|V|Km_K\rangle$ of (3) were made according to the second order of PT (Rajnak and Wybourne 1963, Judd 1967, Demekhin *et al* 1979):

$$\Delta V(Im_I, Km_K)=\sum_{Xm_X}\frac{\langle Im_I|V|Xm_X\rangle\langle Xm_X|V|Km_K\rangle}{E(I)-E(X)}. \tag{5}$$

Equation (5) describes the effective decrease of the Coulomb matrix elements due to many-electron correlations. In the preceding paper (Schmoranzer *et al* 1993) the decrease factor for the $4s^{-1}$–$4p^{-2}nl$ Coulomb interaction was calculated as 1.38 and the decrease factor for the $4p^{-2}nl$–$4p^{-2}n'l'$ Coulomb interaction was estimated as 1.20 as well as the decrease factors of the 4p–4p and 4p–nl Coulomb interactions within the respective configurations.

Spin–orbital interaction for the 4p electron was taken into account by calculating the spin–orbital parameter (Bethe and Salpeter 1957) ξ_{4p}. For the $4p^{-2}4d$ configuration it amounted to $\xi_{4p} = 0.435$ eV.

For the construction of the secular matrices (3) for the total angular momenta $J = \frac{1}{2}, \frac{3}{2}, \frac{5}{2}, \frac{7}{2}$ and $\frac{9}{2}$ in intermediate coupling, the ^2S, $^{2,4}P$, $^{2,4}D$, $^{2,4}F$ and ^2G terms of the ionic configurations listed in table 1 were used. Only even states were included since only these states can be observed by PIFS. After the diagonalization procedure eigenenergies E were obtained as well as eigenvectors $|EJ\rangle$. The eigenvectors $|EJ\rangle$ are of the form

$$|EJ\rangle = \sum_{Im_I} \langle Im_I|EJ\rangle |Im_I\rangle. \tag{6}$$

In (6) $|Im_I\rangle$ denotes the wavefunction of the Im_I state and $\langle Im_I|EJ\rangle$ denotes a numerical eigenvector's coefficient.

2.1.1. Accuracy of energy calculations and reassignment of some levels. The calculated ionic energies of Kr are presented in table 2 together with the data of Moore (1971) and with the percentages of the respective pure basis states in the eigenvectors (6). The agreement of theory and experiment is rather good, in most cases not worse than within a few tens of meV. In some cases, however, the discrepancy between measured and calculated energies is as large as some hundred of meV, e.g. in the case of the $4p^4(^3P)4d\ ^2F_{5/2}$ and $4p^4(^3P)4d\ ^2D_{5/2}$ levels. In this case the assignments of these levels are to some extent conventional because of the complex structure of the respective eigenvectors. The only observable values in the final levels are the ionic energies E and the total ionic momenta J. For example, the most significant components of the eigenvectors mentioned above are the following ($4p^4$ and total momentum J have been omitted on the right-hand side for brevity):

$$\begin{aligned}|E = 30.68\text{ eV}; J = \tfrac{5}{2}\rangle &= 0.36(^3P)4d\ ^2D - \underline{0.83(^3P)4d\ ^2F} - 0.26(^3P)4d\ ^4P \\ &\quad + 0.12(^3P)4d\ ^4F - 0.13(^1S)4d\ ^2D - 0.23(^1D)4d\ ^2D \\ |E = 31.00\text{ eV}; J = \tfrac{5}{2}\rangle &= \underline{0.63(^3P)4d\ ^2D} + 0.48(^3P)4d\ ^2F - 0.11(^3P)4d\ ^4D \\ &\quad - 0.53(^1D)4d\ ^2D + 0.19(^1D)4d\ ^2F + 0.12(^1D)5s\ ^2D.\end{aligned} \tag{7}$$

Therefore we assigned these ionic levels by the largest pure basis $|Im_I\rangle$ states which have been underlined in (7). After reassignment of the levels $|E = 31.00\text{ eV}; J = \frac{5}{2}\rangle$ as $4p^4(^3P)4d\ ^2D_{5/2}$ and $|E = 30.68\text{ eV}; J = \frac{5}{2}\rangle$ as $4p^4(^3P)4d\ ^2F_{5/2}$ the agreement of measured and calculated energies is significantly improved and the deviation does not exceed the average value of a few tens of meV.

The majority of cases where the differences of theory and experiment are larger than the average value is collected in table 3. One can see that after reassignment of these levels the agreement between measured and calculated values is improved. Thus the error of our energy calculations which was estimated as the average experiment–theory deviation is equal to -0.05 ± 0.07 eV. Only the cases of the $4p^4(^1D)4d\ ^2G_{7/2}$ and $4p^4(^1D)4d\ ^2F_{5/2,7/2}$ levels where the differences between theory and experiment are extremely large need additional investigations.

2.1.2. The accuracy of eigenvector calculations. The branching ratios of the radiative decay channels of satellite states into the $4p^5\ ^2P_{3/2}$ and $4p^5\ ^2P_{1/2}$ states as defined by

$$R(EJ)=\frac{I(EJ\rightarrow {}^2P_{3/2})}{I(EJ\rightarrow {}^2P_{1/2})} \tag{8}$$

have been measured previously (Schmoranzer *et al* (1993).

Table 2. Experimental (Moore 1971) and theoretical (this work) energies of even Kr II states.

State		J	Expt E_{exp} (eV)	Theory E_{thy} (eV)	Theory Norm[a] (%)	Diff. $E_{exp}-E_{thy}$ (eV)
$4s^14p^6$	^2S	$\frac{1}{2}$	27.51	27.54	63.6	−0.03
$4p^4(^3P)5s$	^4P	$\frac{5}{2}$	27.99	27.98	95.9	0.01
		$\frac{3}{2}$	28.27	28.24	63.6	0.03
		$\frac{1}{2}$	28.58	28.52	93.0	0.06
$4p^4(^3P)5s$	^2P	$\frac{3}{2}$	28.69	28.63	63.2	0.06
		$\frac{1}{2}$	29.00	28.94	90.5	0.06
$4p^4(^3P)4d$	^4D	$\frac{7}{2}$	28.90	28.94	93.7	−0.04
		$\frac{5}{2}$	28.93	28.98	91.8	−0.05
		$\frac{3}{2}$	29.00	29.05	91.3	−0.05
		$\frac{1}{2}$	29.10	29.13	92.0	−0.03
$4p^4(^3P)4d$	^4F	$\frac{9}{2}$	29.62	29.64	96.0	−0.02
		$\frac{7}{2}$	29.86	29.88	85.8	−0.02
		$\frac{5}{2}$	30.08	30.07	93.7	0.01
		$\frac{3}{2}$	30.09	30.17	96.5	−0.08
$4p^4(^1D)5s$	^2D	$\frac{3}{2}$	29.82	29.82	81.7	0.00
		$\frac{5}{2}$	29.85	29.84	91.2	0.01
$4p^4(^3P)4d$	^4P	$\frac{1}{2}$	30.18	30.25	56.0	−0.07
		$\frac{3}{2}$	30.23	30.30	86.6	−0.07
		$\frac{5}{2}$	30.29	30.46	87.7	−0.17
$4p^4(^3P)4d$	^2F	$\frac{7}{2}$	30.32	30.38	79.3	−0.06
		$\frac{5}{2}$	31.00	30.71	68.9	0.29
$4p^4(^3P)4d$	^2D	$\frac{3}{2}$	30.49	30.73	30.3	−0.24
		$\frac{5}{2}$	30.68	31.02	39.9	−0.34
		$\frac{5}{2}$	30.49			
$4p^4(^3P)4d$	^2P	$\frac{1}{2}$		30.18	29.0	
		$\frac{3}{2}$	30.69	30.57	39.6	−0.12
		$\frac{3}{2}$	31.17			
$4p^4(^1S)5s$	^2S	$\frac{1}{2}$	32.08	32.03	85.2	0.05
$4p^4(^1D)4d$	^2G	$\frac{9}{2}$		31.30	95.9	
		$\frac{7}{2}$	32.21	31.30	91.4	0.93
$4p^4(^1D)4d$	^2D	$\frac{5}{2}$	32.54	32.64	44.9	−0.10
		$\frac{3}{2}$	32.62	32.89	48.3	−0.27
$4p^4(^1D)4d$	^2F	$\frac{7}{2}$	32.58	32.11	93.4	0.47
		$\frac{5}{2}$	32.70	32.02	90.5	0.68
$4p^4(^1D)4d$	^2P	$\frac{3}{2}$	32.82	32.71	43.0	0.11
		$\frac{1}{2}$	32.87	32.92	46.3	−0.05
$4p^4(^3P)6s$	^4P	$\frac{5}{2}$	33.48	33.61	96.4	−0.13
		$\frac{3}{2}$	33.58	34.10	54.2	−0.52
		$\frac{1}{2}$	34.07	34.13	60.2	−0.06
$4p^4(^1D)4d$	^2S	$\frac{1}{2}$		33.93	46.6	
$4p^4(^3P)5d$	^4P	$\frac{1}{2}$	33.94	34.46	51.4	−0.52
		$\frac{3}{2}$	34.01	34.55	61.5	−0.54
		$\frac{5}{2}$	33.96	34.74	50.3	−0.78

Table 2. Continued.

State		J	Expt E_{exp} (eV)	Theory E_{thy} (eV)	Theory Norm[a] (%)	Diff. $E_{exp}-E_{thy}$ (eV)
$4p^4(^3P)5d$	^4D	$\frac{7}{2}$	34.00	34.09	75.6	−0.09
		$\frac{5}{2}$	34.02	34.11	72.3	−0.09
		$\frac{3}{2}$	34.06	34.18	43.1	−0.12
		$\frac{1}{2}$	34.21	34.28	36.2	−0.07
$4p^4(^3P)6s$	^2P	$\frac{3}{2}$	34.09	33.71	68.5	0.38
		$\frac{1}{2}$	34.16	34.24	45.7	−0.08
$4p^4(^3P)5d$	^4F	$\frac{9}{2}$	34.11	34.19	96.4	−0.08
		$\frac{7}{2}$	34.15	34.30	32.4	−0.15
		$\frac{5}{2}$	34.47	34.55	42.2	−0.08
		$\frac{3}{2}$	34.71	34.74	83.2	−0.03
$4p^4(^1S)6s$	^2S	$\frac{1}{2}$	34.39	37.65	67.2	−3.26
$4p^4(^3P)5d$	^2P	$\frac{3}{2}$	34.47	34.92	43.0	−0.45
		$\frac{1}{2}$	34.70	34.79	52.6	−0.09
$4p^4(^3P)5d$	^2F	$\frac{7}{2}$	34.51	34.68	32.4	−0.17
		$\frac{5}{2}$	34.77	34.80	60.4	−0.03
		$\frac{5}{2}$	34.71			
$4p^4(^3P)5d$	^2D	$\frac{3}{2}$	34.82	35.24	27.8	−0.42
		$\frac{5}{2}$	35.04	35.14	53.5	−0.10
$4p^4(^1D)6s$	^2D	$\frac{3}{2}$	35.15	35.43	82.4	
		$\frac{5}{2}$		35.43	88.5	−0.28
$4p^4(^1S)4d$	^2D	$\frac{5}{2}$	35.32	34.03	80.2	1.29
		$\frac{3}{2}$	35.33	34.11	37.1	1.22
$4p^4(^1D)5d$	^2G	$\frac{7}{2}$	35.81	35.95	87.0	−0.14
		$\frac{8}{2}$	35.89	35.94	96.1	−0.05

[a] Square of the largest eigenvector coefficient.

Table 3. Reassignment of Kr II energy levels.

E_{exp} (eV)	J	Moore's (1971) assignment	$E_{exp}-E_{thy}$ (eV)	Present assignment	$E_{exp}-E_{thy}$ (eV)	Norm (%)
30.49	$\frac{3}{2}$	$4p^4(^3P)4d\ ^2D$	−0.24	$4p^4(^3P)4d\ ^2P$	−0.08	39.6
30.69	$\frac{1}{2}$	$4p^4(^3P)4d\ ^2P$	0.12	$4p^4(^3P)4d\ ^2D$	−0.04	30.3
31.00	$\frac{5}{2}$	$4p^4(^3P)4d\ ^2F$	0.29	$4p^4(^3P)4d\ ^2D$	−0.02	39.9
30.68	$\frac{5}{2}$	$4p^4(^3P)4d\ ^2D$	−0.34	$4p^4(^3P)4d\ ^2F$	−0.03	68.9
32.62	$\frac{3}{2}$	$4p^4(^1D)4d\ ^2D$	−0.27	$4p^4(^1D)4d\ ^2P$	−0.09	43.0
32.82	$\frac{3}{2}$	$4p^4(^1D)4d\ ^2P$	0.11	$4p^4(^1D)4d\ ^2D$	−0.07	48.3
33.58	$\frac{3}{2}$	$4p^4(^3P)6s\ ^4P$	−0.52	$4p^4(^3P)6s\ ^2P$	−0.13	68.5
34.09	$\frac{3}{2}$	$4p^4(^3P)6s\ ^2P$	0.38	$4p^4(^3P)6s\ ^4P$	−0.01	54.2
33.94	$\frac{1}{2}$	$4p^4(^3P)5d\ ^4P$	−0.52	$4p^4(^1D)4d\ ^2S$	0.01	46.6
34.01	$\frac{3}{2}$	$4p^4(^3P)5d\ ^4P$	−0.54	$4p^4(^1S)4d\ ^2D$	−0.10	37.1
33.06	$\frac{5}{2}$	$4p^4(^3P)5d\ ^4P$	−0.78	$4p^4(^1S)4d\ ^2D$	−0.07	80.1
34.39	$\frac{1}{2}$	$4p^4(^1S)6s\ ^2S$	−3.26	$4p^4(^3P)5d\ ^4P$	−0.07	51.4
34.47	$\frac{3}{2}$	$4p^4(^3P)5d\ ^2P$	−0.45	$4p^4(^3P)5d\ ^4P$	−0.08	61.5
34.71	$\frac{5}{2}$	—		$4p^4(^3P)5d\ ^4P$	−0.03	50.3
34.82	$\frac{3}{2}$	$4p^4(^3P)5d\ ^2D$	−0.42	$4p^4(^3P)5d\ ^2P$	−0.10	43.0
35.15	$\frac{3}{2}$	$4p^4(^1D)6s\ ^2D$	−0.28	$4p^4(^3P)5d\ ^2D$	−0.09	27.8
35.32	$\frac{5}{2}$	$4p^4(^1S)4d\ ^2D$	1.29	$4p^4(^1D)6s\ ^2D$	−0.11	88.5
35.33	$\frac{3}{2}$	$4p^4(^1S)4d\ ^2D$	1.22	$4p^4(^1D)6s\ ^2D$	−0.10	82.4

The intensities of the radiative transitions are proportional to

$$I(EJ\rightarrow {}^2\mathrm{P}_J)\propto\left|\sum_{Im_l}\langle Im_l|EJ\rangle\langle 4\mathrm{p}^5\,{}^2\mathrm{P}_J|v|Im_l\rangle\right|^2 \tag{9}$$

where v denotes the electric dipole transition operator in velocity form.

It is obvious that the intensity (9) strongly depends on the relative weights $\langle Im_l|EJ\rangle$ of the eigenvector components. Additionally, interference effects between the eigenvector components are present. Thus to calculate $I(EJ\rightarrow {}^2\mathrm{P}_J)$ and $R(EJ)$ very accurate wavefunctions are needed.

Table 4. Calculated and measured branching ratios of radiative decays of Kr II satellite states into the Kr II $4p^5\,{}^2P_{3/2}$ and the Kr II $4p^5\,{}^2P_{1/2}$ states.

Initial state assignment	Branching ratio $^2P_{3/2}:{}^2P_{1/2}$	
	Measured[a]	Theory
$4s^{-1}\,{}^2S_{1/2}$	0.80	0.82
$(^3P)5s\,{}^4P_{1/2}$	0.06	0.0027
$(^3P)5s\,{}^4P_{3/2}$	18.2	15.1
$(^3P)5s\,{}^2P_{3/2}$	5.6	8.89
$(^3P)4d\,{}^4D_{3/2}$	1.9	0.041
$(^3P)5s\,{}^2P_{1/2}$		0.82
$(^3P)4d\,{}^4D_{1/2}$	0.9	0.68

[a] From Schmoranzer *et al* (1993).

$R(EJ)$ values calculated according to (8), (9) are presented in table 4. The good agreement of the calculated $R(EJ)$ values with the measured ones demonstrates the good quality of our eigenvector calculations. The only larger difference between theory and experiment is the case of the $(^3P)4d\,{}^4D_{3/2}$ level. But if it is assumed that the initial state of the fluorescence line in the emission spectrum is to a large extent the $(^3P)5s\,{}^2P_{1/2}$ level the agreement is improved.

2.2. *Photoionization cross section*

The photoionization cross section $\sigma(EJ)$ of the $|EJ\rangle$ levels consists of partial cross sections $\sigma(EJ,\ \varepsilon lsj;\ J=1)$ where ε, l, s, j are the photoelectron quantum numbers and J is the total atomic angular momentum. To calculate $\sigma(EJ)$ one has to sum the partial cross sections over l and j. Summation over j can be done in general yielding for $\sigma(EJ)$:

$$\begin{aligned}\sigma(EJ)&=\sum_{lj}\sigma(EJ,\ \varepsilon lsj;\ J=1)\\&=\frac{4}{3}\frac{\pi^2\alpha a_0^2}{\omega}\sum_{LS,l}\frac{2J+1}{(2L+1)(2S+1)}\\&\quad\times\left|\sum_{Im_{l'}}\delta(S,\tfrac{1}{2})\langle Im_{l'}LS|EJ\rangle\langle Im_{l'}LS\varepsilon l\,{}^1\mathrm{P}|v|0\rangle\right|^2\end{aligned} \tag{10}$$

where the prime on $m_{l'}$ denotes that the total ionic orbital and spin momenta have been extracted from the quantum number set m_l, $|0\rangle$ is the ground state wavefunction, v is the electric dipole operator in velocity form and ω is the energy of the absorbed

photon. The asymptotic behaviour of the continuum state orbitals in equation (10) was normalized to $(2/\pi)^{1/2}\varepsilon^{-1/4}\sin(\sqrt{\varepsilon}\cdot r+\delta)$.

Interference effects are present in (10) only within the *LS* term. Therefore the technique for the calculation of the amplitudes within the module sign is very similar to the *LS* coupling technique used in Sukhorukov *et al* (1991, 1992). To calculate the different amplitudes the following schemes were used.

For the main line:

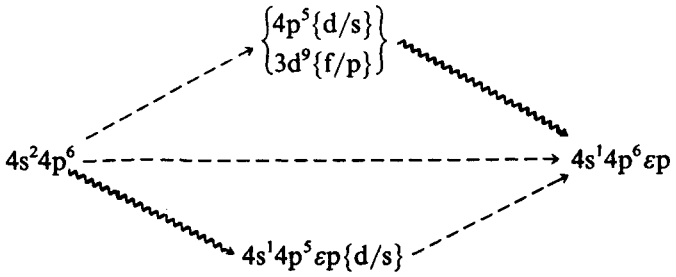

(11)

For the satellite lines:

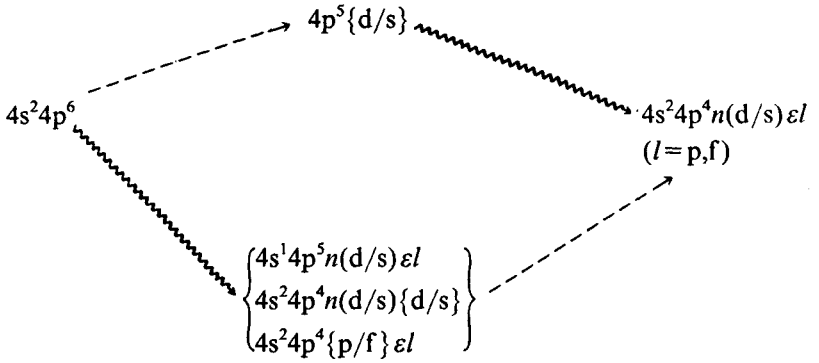

(12)

Here the dashed and wavy lines denote electric dipole and Coulomb interaction, respectively. Summation and integration is performed over the channels shown in curly brackets. These schemes describe direct non-resonant photoionization processes where photoionization through intermediate doubly-excited states of the Kr atom is neglected.

The εp orbitals used in the $\langle 4s|v|\varepsilon p\rangle$ amplitudes have to be calculated in the field of the configurationally mixed state (6). The exact solution of this problem is difficult and exceeds the aim of this paper. However, an additional investigation showed that εp orbitals calculated in a $4s^24p^44d$ core configuration average field or in a $4s^14p^6$ core configuration average field are almost equal. Thus εp orbitals were calculated in the average field of the $4s^24p^44d$ configuration.

The $\langle 4p|v|\{d/s\}\rangle$ amplitudes of (11), (12) were calculated by taking into account inner-shell correlations (Amusia and Cherepkov 1975). The orbitals of the {d/s} channels used in the $\langle 4p|v|\varepsilon'(d/s)\rangle$ amplitudes were calculated by solving (1) in the term-dependent frozen-core approximation for the Kr ground state with an additional 4p vacancy for the term ^{1}P. These ε'd orbitals are non-orthogonal to nd orbitals of the $4p^{-2}nd$ configurations. Therefore the non-orthogonal orbital theory (Jucys and Savukinas 1973) was used to calculate the matrix elements $\langle 4p^{-1}\varepsilon'd|V|4p^{-2}nd\varepsilon l\rangle$ in (12).

In (12) the amplitudes

$$A = \sum_{LS,\varepsilon' > F} \frac{\langle 4p4p\ LS|\, V|nl''\varepsilon' l'\rangle \langle \varepsilon' l'|\, v|\, \varepsilon l\rangle}{-E_{ex} - \varepsilon'} \tag{13}$$

have to be calculated, where $\Sigma_{\varepsilon' > F}$ denotes the summation over unoccupied discrete states nl' and integration over continuum ones and $E_{ex} > 0$ is the energy of the $4p^2 - nl''(\varepsilon' = 0)l'$ excitation (which is in the frozen core approximation equal to $-2\varepsilon_{4p} + \varepsilon_{nl''}$). The involved Coulomb matrix elements have the following form:

$$\langle 4p4p\ LS|\, V|nl''\varepsilon' l'\rangle \equiv \langle 4p^6|\, V|4p^4(LS)nl''\varepsilon' l'\rangle = \sum_k a_k^{LS} R_k(4p4p, nl''\varepsilon' l') \tag{14}$$

where a_k^{LS} are term-dependent coefficients and R_k are Coulomb integrals.

Since the integrals $\langle \varepsilon' l'|\, v|\, \varepsilon l\rangle$ are diverging, the so-called correlation functions

$$\phi_{l''}^{LS} = \sum_{\varepsilon' > F} \frac{\langle 4p4p\ LS|\, V|nl''\varepsilon' l'\rangle}{-E_{ex} - \varepsilon'} |\, \varepsilon' l'\rangle \tag{15}$$

were introduced (see e.g. Carter and Kelly 1977, Sukhorukov *et al* 1992). The radial part $P_{l''}^{LS}(r)$ of the correlation function $\phi_{l''}^{LS}$ is the solution of the following inhomogeneous integro–differential equation

$$(h_{l'}(4p^{-2}nl'') + E_{ex})P_{l''}^{LS}(r) = -\sum_k a_k^{LS}\left[Y_k(4pnl'')P_{4p}(r) - \sum_{n' < F} R_k(4p4p, nl''n'l')P_{n'l'}(r) \right]. \tag{16}$$

In (16) $h_{l'}$ is the same average HF operator as in (1) and a_k^{LS} are the same coefficients as in (14). (16) is obtained by having $(h_{l'}(4p^{-2}nl'') + E_{ex})$ operate on the left- and right-hand sides of (15), performing the integration of the angular part and considering the completeness relation of the $\varepsilon' l'$ set.

With the use of (15), (13) can be rewritten as

$$A = \sum_{LS} < \phi_{l''}^{LS}|\, v|\, \varepsilon l\rangle. \tag{17}$$

(17) does not diverge because of the exponential asymptotic decrease of $P_{l''}^{LS}(r)$.

2.2.1. The strength of the Coulomb interaction. In the previous paper (Schmoranzer *et al* 1993) it was found that correlation effects lead to a significant decrease of the Coulomb interaction, which has influences on the energies of the atomic and ionic states (see also section 2.1), and it was suggested that this decrease has to be considered in transition amplitudes, too.

To check this, the correlational decrease of the $4s\varepsilon'd$–$4p\varepsilon p$ Coulomb interaction was calculated which determines the near-threshold behaviour of the 4s-electron ionization cross section. To determine the corrections to the matrix elements $\langle 4p^5\varepsilon' d\ {}^1P|\, V|4s^1\varepsilon p\ {}^1P\rangle$ the technique described in section 2.1 (see equation (5)) was used. Those intermediate configurations X which influence this matrix element most

Table 5. Correlational corrections to the $\langle 4s^1\varepsilon p\ ^1P|V|4p^5\varepsilon' d\ ^1P\rangle$ matrix element (in per cent).

Intermediate configuration	$\varepsilon = 0.01$ Ryd $\varepsilon' = 0.01$ Ryd	$\varepsilon = 0.01$ Ryd $\varepsilon' = 1.00$ Ryd	$\varepsilon = 0.20$ Ryd $\varepsilon' = 1.00$ Ryd
$4s^14p^5\varepsilon' d\underline{\varepsilon d}$[a]	9.62[b]	6.3	6.8
$4s^14p^4\varepsilon p\varepsilon' d\underline{\varepsilon d}$	7.0	7.5	7.5
$4s^14p^5\underline{\varepsilon s}\varepsilon d$	3.1	3.6	4.5
$3d^94s^14p^5\varepsilon p\varepsilon' d\underline{\varepsilon f}$	1.8	2.7	2.7
$4s^14p^5\underline{\varepsilon d}\varepsilon' d$	1.4	2.1	2.3
$4s^14p^4\varepsilon p\varepsilon' d\underline{\varepsilon s}$	0.4	0.2	0.2
$4s^14p^5\varepsilon p\underline{\varepsilon p}$	0.3	0.3	0.4
$4s^14p^5\varepsilon d\underline{\varepsilon g}$	0.3	0.3	0.4
$3d^94p^5\varepsilon p\underline{\varepsilon f}$	0.3	1.0	1.0
$4s^14p^5\underline{\varepsilon p}\varepsilon f$	0.3	0.4	0.4
$3d^94s^14p^5\varepsilon p\varepsilon' d\underline{\varepsilon p}$	0.2	0.4	0.4
Rest	3.2	2.2	2.5
Total correction	27.9	27.0	29.1
k_2[c]	1.39	1.37	1.41

[a] Integration over the underlined electron states was performed.
[b] Relative values $\Delta V/V$ in per cent.
[c] The second-order factor of the Coulomb interaction correlation decrease (18).

strongly and the respective corrections ΔV (see below) are listed in table 5 for several values of ε and ε'. In the same table, the second-order PT correlation decrease coefficients k_2, which were calculated from

$$\frac{V}{k_2} = V + \Delta V \tag{18}$$

are also presented.

In (18), V and ΔV are the Coulomb matrix element and its correction (5), respectively. Obviously the influence of various intermediate configurations on the matrix element changes slightly with energy but the total effect is approximately constant. Therefore the k_2 value was taken equal to 1.41 for all ε, ε' in the $4s\varepsilon' d$–$4p\varepsilon p$ interactions.

The true correction, however, is overestimated by the second-order PT since the interaction of both initial and final configurations with the intermediate ones should also be decreased by higher-order corrections. This overestimation in the case of 4p4p–4s4d Coulomb interaction was calculated previously (Schmoranzer *et al* 1993) and found to be 1.12. Therefore the coefficient of the correlation decrease of the $4s\varepsilon' d$–$4p\varepsilon p$ Coulomb interaction in our case was assumed to be $k = 1.41/1.12 = 1.26$.

The exact *ab initio* calculation of k, even only for the $4s\varepsilon' d$–$4p\varepsilon p$ interaction, is a very time-consuming procedure, since the application of equation (5) in many cases leads to the integration over two continua. Moreover, the convergence of the sum over the intermediate states X in (5) is very slow (see, e.g., table 5). Thus we used the same value of the Coulomb interaction correlation decrease coefficient $k = 1.26$ for all Coulomb interactions contained in (10), (11) instead of calculating it *ab initio*. The latter task has to be attacked in a forthcoming paper. Some preliminary full *ab initio* calculations support the estimated k value.

3. Results and discussion

3.1. Photoionization cross sections

3.1.1. 4s-electron photoionization cross section. The cross section calculated in velocity form is compared with available measurements and some earlier theoretical data in different energy ranges in figures 1 and 2. Since we found that velocity and length forms usually do not differ by more than 3% we show here the velocity form only. The difference between velocity and length form has its largest value of about 5% around the minimum of the cross section.

The comparison of our earlier calculations (Schmoranzer *et al* 1993) with the present ones (figure 1) shows clearly the effect of the Coulomb interaction decrease: The cross section is decreased considerably in the near-threshold region, suggesting that an improvement could have been obtained in describing the measurements of Schmoranzer *et al* (1993) at energies where there are no resonances (Codling and Madden 1971). However, in view of the large uncertainties of these cross section measurements it is difficult to make a definitive judgement about the degree of agreement between our theoretical and experimental results.

Comparing the present calculations with the earlier ones of Amusia *et al* (1973) and Tulkki *et al* (1992) the following differences have to be pointed out: the minimum of the cross section calculated here lies at a smaller energy than the minimum in the calculations of Amusia *et al* (1973) (figure 2). Recent calculations by Tulkki *et al* (1992) exceed our cross section in the energy region between 60 eV and 90 eV. In this region the calculated cross sections of these authors agree fairly well with the measurements of Aksela *et al* (1987). However, because no uncertainties of these measurements have been quoted, a final judgement about the validity of the approximations used in Tulkki's and our calculations cannot be made at present.

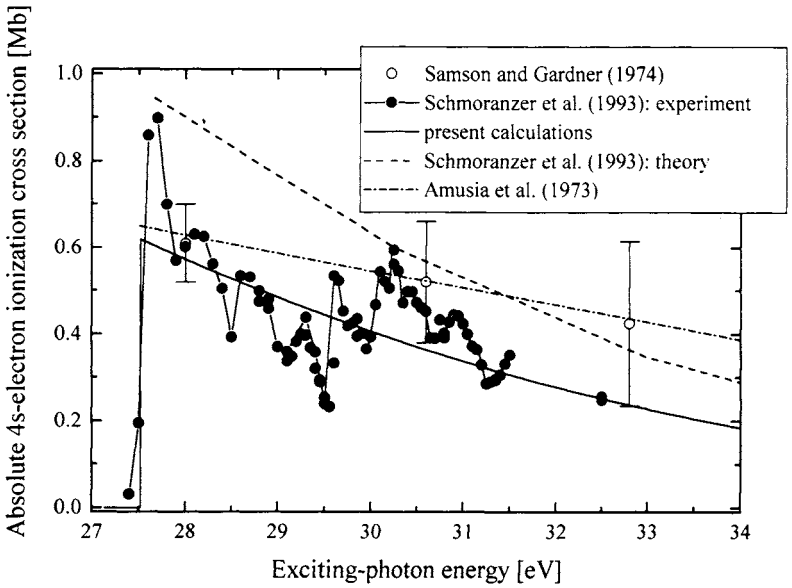

Figure 1. Absolute Kr II 4s-electron photoionization cross section in the near threshold range.

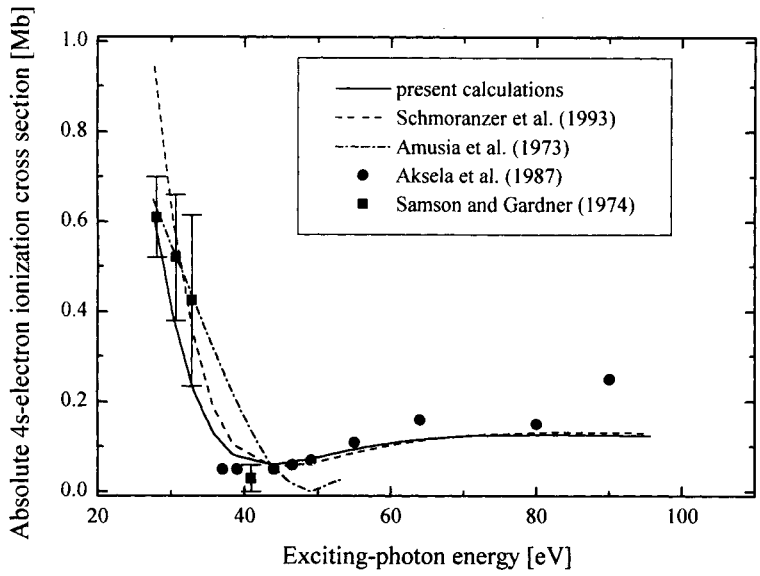

Figure 2. Absolute Kr II 4s-electron photionization cross section in the exciting-photon range between threshold and 90 eV.

3.1.2. Satellite cross sections. Satellite cross sections were calculated for more than a hundred ionic levels with ionic angular momenta $J=\frac{1}{2}$, $\frac{3}{2}$ and $\frac{5}{2}$. In figure 3 those cross sections are presented which may be compared to the measured ones of the preceding paper (Schmoranzer *et al* 1993). Figure 4 shows some of the measured cross sections of Schmoranzer *et al* (1993) together with the calculated ones. However, because resonance effects were not included in the calculations, a comparison can only be made at energies

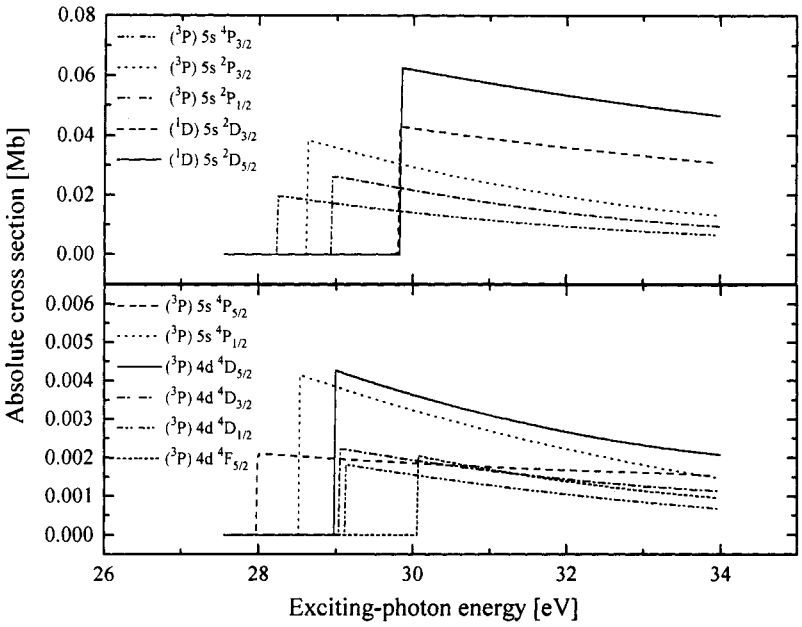

Figure 3. Calculated satellite cross sections for direct photoionization for Kr II levels with threshold energies between 27.51 eV and 30.09 eV.

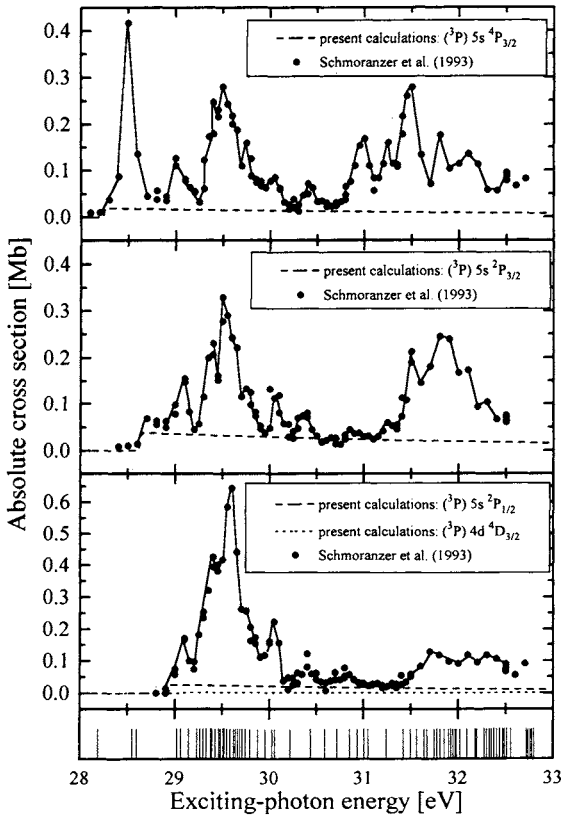

Figure 4. Comparison between calculated and measured photoionization cross sections for some Kr II satellite levels. The bars at the bottom of this figure show the positions of Kr I resonances as measured by Codling and Madden (1971).

where there are no resonances. The positions of these resonances (Codling and Madden 1971) have been marked as bars at the bottom of figure 4. In the cross sections for the $(^3P)5s\ ^4P_{3/2}$ and the $(^3P)5s\ ^2P_{3/2}$ states, the data points between 28.7 eV and 28.9 eV are suited best for a comparison. There seems to be very good agreement between experiment and theory. However, because the experimental data were not recorded at the magic angle (Schmoranzer *et al* 1993) and in view of the large uncertainties of the measurements, a future study of alignment effects with lower uncertainties may modify this result.

The experimental cross section for the level which was assigned $(^3P)4d\ ^4D_{3/2}$ by Hall *et al* (1990) is compared with calculations for the $(^3P)4d\ ^4D_{3/2}$ and the $(^3P)5s\ ^2P_{1/2}$ states. The experimental results fit better with the calculation for the $(^3P)5s\ ^2P_{1/2}$ state in the region between 30.2 eV and 31.4 eV where atomic resonances are rare. This observation supports the result of the radiative branching ratio calculations (see section 2.1.2) where the initial state of the observed fluorescence lines was stated to be, to a large extent, $(^3P)5s\ ^2P_{1/2}$.

3.2. Oscillator strengths of Kr I doubly-excited states

In the previous paper (Schmoranzer *et al* 1993) the calculation of energies and oscillator strengths of Kr doubly-excited states was performed using the *LS*-coupling scheme.

The experiences of these calculations allow us to consider for the present calculation only the most significant states (e.g. the 7p electron was excluded from the present calculation).

The interaction between the np electrons and the core electrons was calculated in the Hartree–Fock approximation. The wavefunctions of the doubly-excited states were constructed as wavefunctions with non-coupling momenta $|EJn\mathrm{p}\rangle$. The energy of such a state was calculated by

$$E(EJn\mathrm{p}) = E(EJ) - \sum_K \left(\sum_{m_k} \langle Km_k | EJ \rangle^2 \mathrm{IP}_k(n\mathrm{p}) \right) \tag{19}$$

where $\langle Km_k|EJ\rangle$ are the same coefficients as in (6). $\mathrm{IP}_k(n\mathrm{p})$ is the ionization potential of the np electron in the configuration K. The ionization potentials were calculated by including many-body effects as described in Schmoranzer *et al* (1993). They are listed in table 6.

Table 6. Ionization potentials in (eV) of np electrons calculated in different configurations.

K	IP_K(5p)	IP_K(6p)
$4s^{-1}$	2.58	1.19
$4p^{-2}$ 4d	2.83	1.28
5d	4.61	1.63
6d	5.64	2.06
7d	6.19	2.72
8d	6.53	3.03
5s	3.24	1.28
6s	4.48	1.69

The oscillator strengths f for the transitions into the doubly-excited states were calculated analogously to the photoionization cross sections σ by replacing in the schemes (11) and (12) εp and εl by the two bound outer electrons and by using the relation $\sigma = 2\pi^2 \alpha a_0^2 f$ (see Schmoranzer *et al* 1993). The calculated energies and oscillator strengths are shown in table 7.

A comparison between the present results and the earlier ones of Schmoranzer *et al* (1993) reveals two main differences.

(i) The total oscillator strengths decreased by a factor of 1.81 as compared to the earlier work resulting in a value of 0.106 au. This decrease is caused by the correlational decrease of the Coulomb interaction (see section 2.2.1).

(ii) The appearance of transitions into states genealogically connected with quartet core states is due to the spin–orbital interaction of the 4p electrons. This interaction causes also a splitting of the doubly-excited states, i.e. more doubly-excited states appear than in the calculation without spin–orbital interaction.

The data of table 7 lead to the following qualitative interpretation of some features in the satellite cross sections in the exciting-photon energy range between 28 eV and 30 eV (see figure 4).

(i) The sharp peak at 28.5 eV is connected with the $4p^4(^1S)5s(^2S_{1/2})5p$ and $4p^4(^1D)5s(^2D_{3/2,5/2})6p$ states.

(ii) The broad structure between 29 eV and 30 eV is connected with the $4p^4(^1D)4d(^2P_{1/2,3/2})5p$ and $4p^4(^1D)4d(^2D_{3/2,5/2})5p$ states.

However, this interpretation may be slightly changed after considering the Coulomb interaction of the np electrons with the ionic core which has been omitted in the present calculation. This interaction will lead to an additional mixing of the ionic states.

Table 7. Energies, genealogy and oscillator strengths of transitions into doubly-excited states of Kr, calculated in intermediate coupling.

Core term $J=\frac{1}{2}$				Core term $J=\frac{3}{2}$				Core term $J=\frac{5}{2}$			
Configuration		Photon energy (eV)	f ($\times 10^{-3}$)	Configuration		Photon energy (eV)	f ($\times 10^{-3}$)	Configuration		Photon energy (eV)	f ($\times 10^{-3}$)
$4s^{-1}(^2S)$	5p	24.84	22.44	$4p^4(^3P)5s(^4P)$	5p	25.01	0.99	$4p^4(^1D)5s(^2D)$	5p	26.63	2.93
64%[a]	6p	26.32	5.28	64%	6p	26.96	0.17	91%	6p	28.56	0.60
$4p^4(^3P)5s(^2P)$	5p	25.71	1.34	$4p^4(^3P)5s(^2P)$	5p	25.39	1.93	$4p^4(^1D)4d(^2D)$	5p	29.51	6.97
90%	6p	27.65	0.22	63%	6p	27.35	0.34	45%	6p	31.30	1.29
$4p^4(^1S)5s(^2S)$	5p	28.82	8.04	$4p^4(^1D)5s(^2D)$	5p	26.64	1.98	$4p^4(^1S)4d(^2D)$	5p	30.99	1.98
85%	6p	30.75	1.56	82%	6p	28.54	0.42	80%	6p	32.71	0.40
$4p^4(^1D)4d(^2P)$	5p	29.73	5.58	$4p^4(^1D)4d(^2P)$	5p	29.57	11.14	$4p^4(^3P)5d(^4F)$	5p	30.02	1.07
46%	6p	31.56	1.12	43%	6p	31.36	2.26	42%	6p	32.93	0.15
$4p^4(^1D)4d(^2S)$	5p	30.66	11.33	$4p^4(^1D)4d(^2D)$	5p	29.81	3.67	$4p^4(^3P)5d(^2D)$	5p	30.56	2.36
47%	6p	32.57	2.13	48%	6p	31.55	0.69	54%	6p	33.48	0.32
$4p^4(^1D)5d(^2S)$	5p	31.96	5.43								
66%	6p	34.86	0.84								

[a] Percentage of the pure basis state in the doubly-excited state eigenvector.

For a further detailed comparison with experiment, the calculation of the branching ratio between the decays of the doubly-excited states into the Kr II ground state, the Kr II $4s^14p^6\ ^2S_{1/2}$ state and the Kr II satellite states as well as the calculation of the interference profiles (Fano 1961, Combet-Farnoux 1982) is necessary which have not been carried out in this work.

4. Summary

Many-body calculations were performed for the Kr II ionic energy structure at an accuracy level of approximately 0.05 eV which was sufficient to suggest reassignments of some even Kr II levels identified previously by Moore (1971). Many-body calculations were performed also for the branching ratio of the fluorescent decays of some Kr II satellite states into the Kr II $4s^24p^5\ ^2P_{1/2}$ and $^2P_{3/2}$ ground states. A comparison with recent measurements (Schmoranzer *et al* 1993) gives satisfactory agreement.

The effect of higher-order PT corrections on the cross section calculations was investigated and it was shown that higher-order PT corrections decrease the Coulomb interaction which determines the near-threshold cross section values. The photoionization cross sections calculated by taking into account the higher-order PT corrections were found to be in good agreement with measurements for both main and satellite levels.

Acknowledgments

This work has been funded by the German Federal Minister for Research and Technology under contract no 05 5UKAXB. VLS and BML gratefully acknowledge support

by the Sonderforschungsbereich 91 of the Deutsche Forschungsgemeinschaft during their stay at Kaiserslautern.

References

Aksela S, Aksela H, Levasalmi M, Tan K H and Bancroft G M 1987 *Phys. Rev.* A **36** 3449–50

Amusia M Ya and Cherepkov N A 1975 *Case Stud. At. Phys.* **5** 47–121

Amusia M Ya, Ivanov V K, Cherepkov N A and Chernysheva L V 1973 *Proc. 8th Int. Conf. on Physics of Electronic and Atomic Collisions (Belgrade)* (Amsterdam: North-Holland) Abstracts p 581–2

Bethe H and Salpeter E 1957 *Quantum Mechanics of One- and Two-Electron Atoms* (Berlin: Springer)

Carter S L and Kelly H P 1977 *Phys. Rev.* A **16** 1525–34

Codling K and Madden R P 1971 *J. Res. NBS* A **76** 1–12

Combet-Farnoux F 1982 *Phys. Rev.* A **25** 287–303

Demekhin V F, Sukhorukov V L, Shelkovich T V, Yavna S A, Yavna V A and Bairachny Yu I 1979 *J. Struct. Chem. (USSR)* **20** 28–48

Fano U 1961 *Phys. Rev.* **124** 1866–78

Hall R I, Dawber G, Ellis K, Zubek M, Avaldi I and King G C 1990 *J. Phys. B: At. Mol. Opt. Phys.* **24** 4133–46

Jucys A P and Savukinas A J 1973 *Mathematical Foundations of the Atomic Theory* (Vilnius: Mintis)

Judd B R 1967 *Second Quantization and Atomic Spectroscopy* (Baltimore, MD: Hopkins)

Moore C E 1971 *Atomic Energy Levels* (NBS Circular No 467) (Washington, DC: US Govt Printing Office)

Rajnak K and Wybourne B G 1963 *Phys. Rev.* **132** 280–90

Petrov I D and Sukhorukov V L 1991 *Today and Tomorrow in Photionization* ed M Ya Amjusia and J B West (DL/SCI/R29 Daresbury Laboratory) p 187

Samson J A R and Gardner J L 1974 *Phys. Rev. Lett.* **33** 671–3

Schmoranzer H, Ehresmann A, Vollweiler F, Sukhorukov V L, Lagutin B M, Petrov I D, Schartner K H and Möbus B 1993 *J. Phys B: At. Mol. Opt. Phys.* **26** 2795–810 (Corrigendum 1994 *J. Phys. B: At. Mol. Opt. Phys.* **27** 377–9

Schmoranzer H, Wildberger M, Schartner K H, Möbus B and Magel B 1990 *Phys. Lett.* **150A** 281–5

Sukhorukov V L, Lagutin B M, Schmoranzer H, Petrov I D and Schartner K H 1992 *Phys. Lett.* **169A** 445–51

Sukhorukov V L, Petrov I D, Lavrent'ev S V and Demekhin V F 1991 *Today and Tomorrow in Photionization* ed M Ya Amusia and J B West (DL/SCI/R29 Daresbury Laboratory) p 7

Tulkki J, Aksela S, Aksela H, Shigemasa E, Yagishita A and Furusawa Y 1992 *Phys. Rev.* A **45** 4640–5